9-4-2018

Two-dimensional type-II Dirac fermions in a LaAlO3/LaNiO3/LaAlO3 quantum well

L. L. Tao
University of Nebraska-Lincoln, ltao2@unl.edu

Evgeny Y. Tsymbal
University of Nebraska-Lincoln, tsymbal@unl.edu

Rapid Communications

Two-dimensional type-II Dirac fermions in a $LaAlO_3/LaNiO_3/LaAlO_3$ quantum well

L. L. Tao* and Evgeny Y. Tsymbal†

Department of Physics and Astronomy & Nebraska Center for Materials and Nanoscience, University of Nebraska, Lincoln, Nebraska 68588, USA

(Received 16 July 2018; published 4 September 2018)

The type-II Dirac fermions that are characterized by a tilted Dirac cone and anisotropic magnetotransport properties have been recently proposed theoretically and confirmed experimentally. Here, we predict the emergence of two-dimensional (2D) type-II Dirac fermions in $LaAlO_3/LaNiO_3/LaAlO_3$ quantum-well structures. Using first-principles calculations and model analyses, we show that the Dirac points are formed at the crossing between the $d_{x^2-y^2}$ and d_{z^2} bands protected by the mirror symmetry. The energy position of the Dirac points can be tuned to appear at the Fermi energy by changing the quantum-well width. For the quantum-well structure with a two-unit-cell-thick $LaNiO_3$ layer, we predict the coexistence of the type-II Dirac point and the closed nodal line. The results are analyzed and interpreted using a tight-binding model and symmetry arguments. Our findings offer a practical way to realize 2D type-II Dirac fermions in oxide heterostructures.

DOI: 10.1103/PhysRevB.98.121102

Introduction. The recent proposal of type-II Weyl fermions [1] has inspired intensive investigations of the counterpart type-II Dirac fermions [2–5]. The type-II Weyl/Dirac fermions merge at the boundary between electron and hole pockets and exhibit specific anisotropic magnetotransport behavior qualitatively different from the type-I Dirac fermions [1,6,7]. To date, a handful of candidates hosting three-dimensional (3D) type-II Dirac fermions have been theoretically proposed, such as materials deriving from the $PtSe_2$ [2], YPd_2Sn [3], VAl_3 [4], and KMnBi [5] families. The experimental evidence for 3D type-II Dirac fermions in bulk $PtSe_2$ [8,9], $PtTe_2$ [10], and $PdTe_2$ [11] has been reported based on angle-resolved photoemission spectroscopy measurements.

On the other hand, towards the device miniaturization, it would be beneficial to realize type-II Dirac fermions in two-dimensional (2D) systems by analogy to the well-known type-I Dirac fermions in graphene [12]. For example, the existence of 2D type-II Dirac fermions has been predicted in monolayer WTe_2 [13], graphene with nitrogen line defects [14], and quinoid-type α-$(BEDT\text{-}TTF)_2I$ [15]. However, the properties of these free-standing 2D material systems may change when they are deposited on a substrate to perform experimental measurements. For example, the Dirac cone in a free-standing silicene is destroyed due to the hybridization with an Ag(111) substrate [16]. In this regard, it would be desirable to find 2D systems, which can be accurately controlled and not affected by the conditions of measurements. From this point of view, complex oxide heterostructures may serve as a fertile playground to realize 2D type-II Dirac fermions in practice. Due to advances in thin-film deposition and characterization techniques, layered oxide heterostructures can be synthesized with atomic-scale precision, and they exhibit a variety of electronic phenomena not found in the bulk constituents [17]. Very recently, 2D type-II Dirac fermions have been observed in a layered oxide $La_{2-x}Sr_xCuO_4$ [18].

Here, we propose the realization of 2D type-II Dirac fermions in the experimentally feasible oxide quantum-well structures $LaAlO_3/LaNiO_3/LaAlO_3(001)$ [19]. Bulk $LaNiO_3$ (LNO) is a paramagnetic metal [20,21], which can be used as an oxide electrode [22,23], while bulk $LaAlO_3$ (LAO) is a wide-gap insulator [24]. Previous work on LNO/LAO (001) heterostructures has been focused on orbital engineering to produce novel electronic properties [25–28]. Here, we exploit the effect of quantum confinement of the LNO layer to form the emerging electronic states. We predict that type-II Dirac points (DPs) appear along the diagonal axes of the 2D Brillouin zone (BZ) and the band dispersion around the DP is strongly anisotropic in the momentum space. Given the experimentally feasible structure with tunable degrees of freedom, the proposed LAO/LNO/LAO quantum-well system represents a promising candidate to realize 2D type-II Dirac fermions in practice.

Results and discussion. First, we investigate the atomic and electronic structure of a $LAO/(LNO)_n/LAO$ quantum well with LNO thickness n of 1.0 unit cell (u.c.), as depicted in Fig. 1(a). Density-functional theory (DFT) calculations are performed using the plane-wave ultrasoft pseudopotential method [29] implemented in QUANTUM ESPRESSO [30–33] (further details can be found in the Supplemental Material [34]). Figure 1(b) shows the calculated relative metal-oxygen (M-O) displacements across the heterostructure. Overall, we see that the displacements are quite small with a slight enhancement $\sim$0.03 Å at the interfaces. This stems from no electrostatic mismatch across the interface, due to the equal formal valence of the $(NiO_2)^-$ and $(AlO_2)^-$ atomic layers. This is in contrast to the well-known $SrTiO_3/LaAlO_3$ (001) system where a large La-O displacement at the interface $\sim$0.2 Å is produced between the charged $(LaO)^+$ and neutral $(TiO_2)^0$ atomic layers [35]. Figure 1(c) shows the local density of states (LDOS) across the quantum well. It

*ltao2@unl.edu
†tsymbal@unl.edu

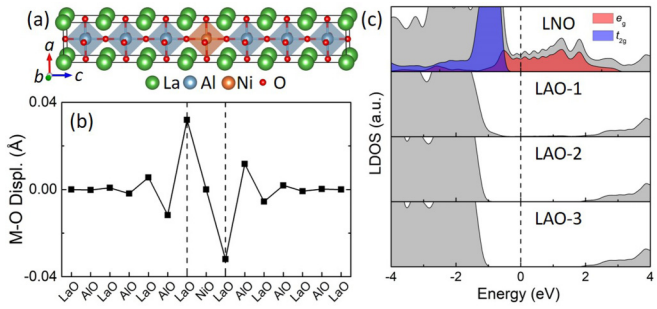

FIG. 1. (a) Atomic structure of the LAO/$(LNO)_1$/LAO quantum well. Here (a, b, c) axes are concordant with the (x, y, z) axes. (b) The relative metal-O (M-O) displacements. The two vertical dashed lines denote the interfaces. (c) Local density of states (LDOS) on layers from LNO to deep LAO-3. The vertical dashed line denotes the Fermi energy.

is seen that the LDOS at the Fermi energy E_F is nonzero only within the LNO layer, suggesting a nearly perfect 2D electron gas. Examining the LDOS of the LNO layer suggests that the Ni-t_{2g}(d_{xy}, d_{yz}, d_{zx}) orbitals are well below E_F and fully occupied, whereas the Ni-e_g ($d_{x^2-y^2}$, d_{z^2}) orbitals are partially occupied and thus determine the electronic structure around E_F.

Next, we discuss the electronic structure of the LAO/$(LNO)_1$/LAO quantum well. Figure 2(a) shows the calculated band structure without spin-orbit coupling (SOC). It is seen that the $d_{x^2-y^2}$ and d_{z^2} bands cross each other along the Γ-M line. Zooming in around the crossing point (∼0.8 eV above E_F) reveals a linear dispersion, which

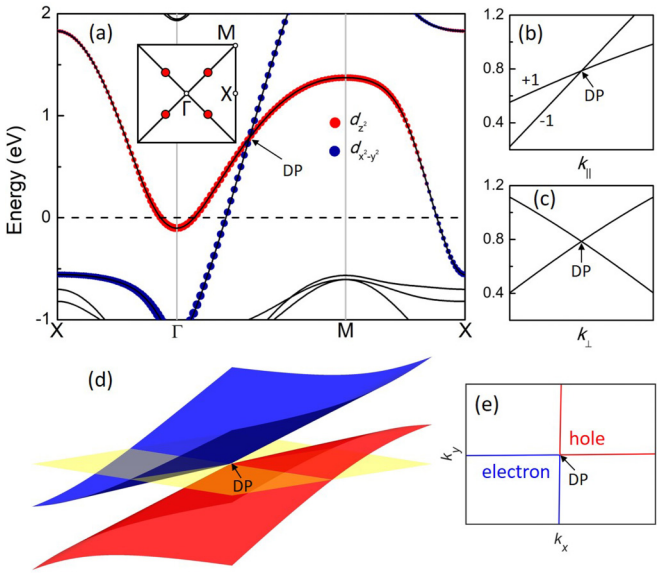

FIG. 2. (a) Band structure of the LAO/$(LNO)_1$/LAO quantum well along the high symmetry lines $X(\pi,0)$-$\Gamma(0,0)$-$M(\pi,\pi)$-$X(\pi,0)$ without SOC. Projection onto the e_g ($d_{x^2-y^2}$, d_{z^2}) orbitals is indicated by dots whose sizes correspond to the weight of each orbital. Inset: The 2D BZ. Positions of DPs are indicated by the red dots. Zoom-in band structure around the DP (b) along Γ-M ($k_\parallel$) and (c) perpendicular to Γ-M ($k_\perp$). (d) 3D band structure around the DP. (e) Energy contour for the isoenergy cutting [yellow plane in (d)] through the DP.

is strongly anisotropic in k space [Figs. 2(b) and 2(c)]. The band crossing is tilted along Γ-M [Fig. 2(b)], while it is straight perpendicular to Γ-M [Fig. 2(c)]. Figure 2(d) shows the 3D band structure around the crossing point. It is seen that cutting the bands by the isoenergy plane opens electron and hole pockets touching at the crossing point [Fig. 2(e)]. Due to space inversion symmetry P and time-reversal symmetry T, each band represents a Kramers doublet which makes the crossing point fourfold degenerate. These properties are the characteristic features of a type-II Dirac fermion and the crossing point is the well-known DP. Due to the C_4 fourfold rotation symmetry, there are four equivalent DPs in the 2D BZ [red dots in the inset of Fig. 2(a)]. The type-II DP due to the unavoidable crossing between the two e_g bands has been also found in the bulk cuprate oxides [18].

The DPs are protected by the mirror symmetry. Along Γ-M, wave vector $\mathbf{k}$ is invariant under the symmetry operation M_{xy} perpendicular to the $k_y = -k_x$ axis. In the spinless case, $M_{xy}^2 = 1$ and hence bands along Γ-M can be characterized by the eigenvalues (± 1) of M_{xy}. It is evident that $M_{xy}|d_{x^2-y^2}\rangle = -|d_{x^2-y^2}\rangle$ and $M_{xy}|d_{z^2}\rangle = -|d_{z^2}\rangle$ (here $|\cdots\rangle$ denotes the orbital basis). The different eigenvalues (different irreducible representations) forbid hybridization between the $d_{x^2-y^2}$ and d_{z^2} bands. The DP is therefore protected by M_{xy} symmetry and cannot be gapped.

To gain further insight into the nature of the DP, we derive the $\mathbf{k}\cdot\mathbf{p}$ effective Hamiltonian based on the theory of invariants [36–38]. The Hamiltonian up to the linear order in q is given by [34]

$$H = \alpha_1(q_x + q_y)\sigma_0 + \beta_1(q_x - q_y)\sigma_x + \gamma_1(q_x + q_y)\sigma_z, \quad (1)$$

where (q_x, q_y) is the wave-vector deviations from the DP and (α_1, β_1, γ_1) are expansion coefficients, σ_0 is the 2×2 unitary matrix, and (σ_x, σ_z) are the Pauli matrices acting within the orbital space. The energy spectrum of Eq. (1) is

$$\varepsilon_\pm = \alpha_1(q_x + q_y) \pm \sqrt{\beta_1^2(q_x - q_y)^2 + \gamma_1^2(q_x + q_y)^2}. \quad (2)$$

Equation (2) describes the 2D anisotropic massless Dirac fermions. Fitting to the band around the DP yields $\alpha_1 = 2.33$ eV Å, $\beta_1 = 2.13$ eV Å, and $\gamma_1 = 1.03$ eV Å. Along Γ-M, $q_x = q_y$ and the Dirac cone is strongly titled due to $\alpha_1 > \gamma_1$.

We see that the LAO/$(LNO)_1$/LAO hosts 2D type-II Dirac fermions due to the symmetry protected band crossing between the two e_g bands. However, the energy position of the DP is relatively high, i.e., ∼0.8 eV above E_F. Electron doping or gate biasing are technically feasible to tune the DP closer to E_F. However, there is another efficient way to tune the DP by changing the quantum-well width (LNO layer thickness) [34].

Figure 3(a) shows the calculated band structure of the LAO/$(LNO)_2$/LAO (001). A comparison to Fig. 2(a) reveals that the quantum confinement in the z direction splits the two d_{z^2} bands: at the Γ point, one band shifts above E_F while the other band moves below E_F. On the other hand, the dispersion of the $d_{x^2-y^2}$ bands is nearly unaffected due to the $d_{x^2-y^2}$ orbitals lying in the xy plane. As a result, the two crossing points between the lower d_{z^2} band and the two $d_{x^2-y^2}$ bands become closer to E_F. These crossing points, denoted by P and Q, are seen in Fig. 3(b) along Γ-M ($k_\parallel$). Figures 3(c) and 3(d) show the band dispersions perpendicular to Γ-M ($k_\perp$) and

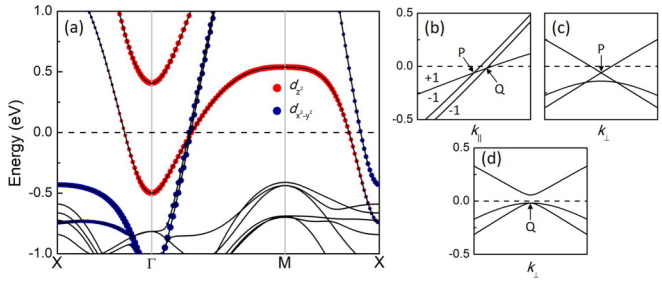

FIG. 3. (a) Band structure of the LAO/$(LNO)_2$/LAO quantum well without SOC. Projection onto the e_g ($d_{x^2-y^2}$, d_{z^2}) orbitals is indicated by dots whose sizes correspond to the weight of each orbital. Zoom-in band structure around crossing points (b) along Γ-M ($k_\parallel$) and (c), (d) perpendicular to Γ-M ($k_\perp$) passing through (c) P and (d) Q points.

passing through the P and Q points, respectively. It is seen that the P point exhibits properties similar to the DP in the LAO/$(LNO)_1$/LAO: a linear dispersion in all directions, the titled band crossing along $k_\parallel$ [Fig. 3(b)], and the straight band crossing along $k_\perp$ [Fig. 3(c)]. The Q point reveals, however, a different behavior: along $k_\parallel$, the crossing bands have the titled linear dispersion [Fig. 3(b)], while along $k_\perp$, the dispersion is quadratic [Fig. 3(d)]. Using a tight-binding (TB) model (discussed below), we have calculated the band dispersion around E_F. Figure 4(a) shows that the P point emerges as an isolated point, while the Q point belongs to a closed nodal line (NL). It is evident from Fig. 4(b) that the energy of the NL varies from −0.04 to −0.7 eV, which favors the experimental measurement over a large energy scale.

The NL appears due to the PT symmetry, which in general produces a closed nodal loop in the BZ [39–41]. The point group for a arbitrary crossing point at the NL is C_s, which consists of the identity element E and the mirror reflection M_z with respect to the plane perpendicular to the z axis. There are two irreducible representations of the C_s group [42], A' and A''. Examining the two bands forming the NL [Fig. S5(a)], we find that one band belongs to the A' representation, while the other one belongs to the A'' representation [34]. Since the

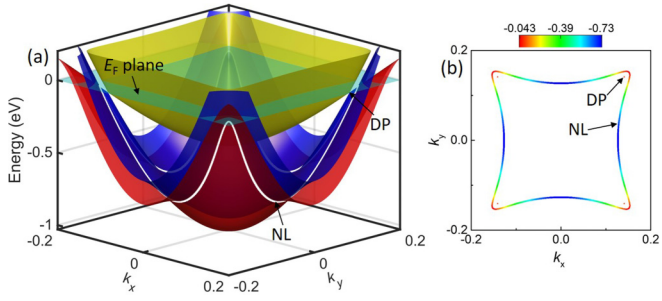

FIG. 4. (a) 3D plot of the band structure around the Fermi energy. Band touching points between red and blue branches form the closed node line (NL), as indicated by white loop. (b) 2D projection of the isolated DPs and the closed NL. k_x and k_y are in units of $2\pi/a$. The color map quantifies the band energies at the touching points. The results are obtained using the tight-binding Hamiltonian model as described in the text.

eigenvalue of M_z for the A' (A'') representation is +1 (–1) [42,43], the NL is protected by the mirror symmetry M_z.

To obtain a deeper insight into the band structure of the LAO/LNO/LAO, we construct a TB Hamiltonian in the basis of the $|d_{x^2-y^2}\rangle$ and $|d_{z^2}\rangle$ orbitals, which are denoted as $|\alpha\rangle$ and $|\beta\rangle$, respectively. The Hamiltonian model and energy spectrum can be found in the Supplemental Material [34]. Along Γ-M ($k_x = k_y$), the band energies are $\varepsilon_\pm = h_\beta, h_\alpha$ for 1-u.c.-thick LNO and $\varepsilon_{1,4} = h_\beta \mp h_{\beta z}$, $\varepsilon_{2,3} = h_\alpha \mp h_{\alpha z}$ for 2-u.c.-thick LNO [Supplemental Eqs. (5) and (12)], where h's are the functions of (k_x, k_y). In the latter case, both h_α and h_β are split into two subbands with the splitting energy being proportional to $2h_{\alpha z}$ and $2h_{\beta z}$, respectively. Since the $|\alpha\rangle$ ($|\beta\rangle$) orbital lies in (out of) the plane, the out-of-plane hopping $h_{\alpha z}$ is expected to be much smaller than $h_{\beta z}$, which is confirmed by the fitting [34]. Consequently, the splitting between the two d_{z^2} bands is significantly larger than the splitting between the two $d_{x^2-y^2}$ bands, which is in line with our DFT results [Fig. 3(a)].

It is noteworthy that the previous experimental work [44,45] has demonstrated a metal-insulator transition (MIT) in a few-u.c.-thick LNO film due to the low dimensionality and strain. However, very recently it was demonstrated that oxygen vacancies play a critical role in triggering the MIT [46]. Moreover, both the DFT and DFT+DMFT (dynamical mean-field theory) results reveal the metallic feature even for 1-u.c.-thick LNO film without oxygen vacancies [46], in agreement with our results.

Finally, we discuss the effect of SOC on the DPs from symmetry arguments. Here, we consider a LAO/$(LNO)_1$/LAO as an example, but the same conclusion applies to LAO/$(LNO)_2$/LAO as well. Along Γ-M, there are two symmetry invariant operations, i.e., PT and M_{xy}. In real space, it can be easily checked that $[PT, M_{xy}] = 0$. In spin space, we have $PT = i\sigma_y K$ and $M_{xy} = i(\sigma_x - \sigma_y)/\sqrt{2}$. Combining real and spin spaces, we obtain $[PT, M_{xy}] = 0$ and $M_{xy}^2 = -1$. Along Γ-M, the Bloch states $|\psi\rangle$ and $PT|\psi\rangle$ can be labeled using the eigenvalues of M_{xy}, namely, $M_{xy}|\psi\rangle = \pm i|\psi\rangle$ and $M_{xy}PT|\psi\rangle = \mp iPT|\psi\rangle$. The doubly degenerate states $|\psi\rangle$ and $PT|\psi\rangle$ have opposite M_{xy} eigenvalues. Therefore, when two sets of such doublet bands cross at the DP, the two bands with the same M_{xy} eigenvalue can hybridize and open a gap at the DP, as schematically shown in Figs. S3(b) and S3(c). To confirm this, we have calculated the band structure by including SOC. As shown in the Fig. S4, a tiny gap of ∼2 meV appears at the DP. Thus, in the spinful case, the DP is not protected by the mirror symmetry and a small gap opens due to SOC. The same conclusion also applies to the NL [Fig. S5(b)].

Summary. In summary, we have predicted that the LAO/LNO/LAO (001) quantum-well structures host 2D type-II Dirac fermions. Our DFT calculations and TB modeling demonstrate that a 1-u.c.-thick LNO layer, when placed in the quantum well, forms the Dirac points that are located along the diagonal lines of the 2D Brillouin zone and in the spinless case are protected by the mirror symmetry. The formation of the 2D type-II Dirac fermions can be tuned by the quantum-well width. Moreover, growing LAO/LNO/LAO on different substrates [19,47] enables the strain-tunable DP [34]. For a 2-u.c.-thick LNO layer, the energy position of the Dirac point is

found to appear near the Fermi energy. In this case, we predict the coexistence of the isolated Dirac points and a closed nodal line. SOC opens a small (∼2-meV) gap at the Dirac points and the nodal line. We hope that our findings will stimulate the experimental search for 2D type-II Dirac fermions in the LAO/LNO/LAO (001) quantum-well structures.

This work was supported by the National Science Foundation (NSF) through Nebraska Materials Research Science and Engineering Center (MRSEC) (NSF Grant No. DMR-1420645). Computations were performed at the University of Nebraska Holland Computing Center. The atomic structure was produced using VESTA software [48].

[1] A. A. Soluyanov, D. Gresch, Z. Wang, Q. Wu, M. Troyer, X. Dai, and B. A. Bernevig, Nature (London) **527**, 495 (2015).
[2] H. Huang, S. Zhou, and W. Duan, Phys. Rev. B **94**, 121117(R) (2016).
[3] P. J. Guo, H. C. Yang, K. Liu, and Z. Y. Lu, Phys. Rev. B **95**, 155112 (2017).
[4] T. R. Chang, S. Y. Xu, D. S. Sanchez, W. F. Tsai, S. M. Huang, G. Chang, C. H. Hsu, G. Bian, I. Belopolski, Z. M. Yu, S. A. Yang, T. Neupert, H. T. Jeng, H. Lin, and M. Z. Hasan, Phys. Rev. Lett. **119**, 026404 (2017).
[5] C. Le, S. Qin, X. Wu, X. Dai, P. Fu, C. Fang, and J. Hu, Phys. Rev. B **96**, 115121 (2017).
[6] Z. M. Yu, Y. Yao, and S. A. Yang, Phys. Rev. Lett. **117**, 077202 (2016).
[7] S. Tchoumakov, M. Civelli, and M. O. Goerbig, Phys. Rev. Lett. **117**, 086402 (2016).
[8] K. Zhang, M. Yan, H. Zhang, H. Huang, M. Arita, Z. Sun, W. Duan, Y. Wu, and S. Zhou, Phys. Rev. B **96**, 125102 (2017).
[9] Y. Li, Y. Xia, S. A. Ekahana, N. Kumar, J. Jiang, L. Yang, C. Chen, C. Liu, B. Yan, C. Felser, G. Li, Z. Liu, and Y. Chen, Phys. Rev. Mater. **1**, 074202 (2017).
[10] M. Yan, H. Huang, K. Zhang, E. Wang, W. Yao, K. Deng, G. Wan, H. Zhang, M. Arita, and H. Yang, Nat. Commun. **8**, 257 (2017).
[11] H.-J. Noh, J. Jeong, E.-J. Cho, K. Kim, B. I. Min, and B.-G. Park, Phys. Rev. Lett. **119**, 016401 (2017).
[12] A. H. Castro Neto, F. Guinea, N. M. R. Peres, K. S. Novoselov, and A. K. Geim, Rev. Mod. Phys. **81**, 109 (2009).
[13] L. Muechler, A. Alexandradinata, T. Neupert, and R. Car, Phys. Rev. X **6**, 041069 (2016).
[14] H. Zhang, Y. Xie, C. Zhong, Z. Zhang, and Y. Chen, J. Phys. Chem. C **121**, 12476 (2017).
[15] M. O. Goerbig, J.-N. Fuchs, G. Montambaux, and F. Piéchon, Phys. Rev. B **78**, 045415 (2008).
[16] Y. P. Wang and H. P. Cheng, Phys. Rev. B **87**, 245430 (2013).
[17] H. Y. Hwang, Y. Iwasa, M. Kawasaki, B. Keimer, N. Nagaosa and Y. Tokura, Nat. Mater. **11**, 103 (2012).
[18] M. Horio, C. E. Matt, K. Kramer, D. Sutter, A. M. Cook, Y. Sassa, K. Hauser, M. Månsson, N. C. Plumb, M. Shi, O. J. Lipscombe, S. M. Hayden, T. Neupert, and J. Chang, Nat. Commun. **9**, 3252 (2018).
[19] F. Wrobel, A. F. Mark, G. Christiani, W. Sigle, H.-U. Habermeier, P. A. van Aken, G. Logvenov, B. Keimer, and E. Benckiser, Appl. Phys. Lett. **110**, 041606 (2017).
[20] M. L. Medarde, J. Phys.: Condens. Matter **9**, 1679 (1997).
[21] G. Gou, I. Grinberg, A. M. Rappe, and J. M. Rondinelli, Phys. Rev. B **84**, 144101 (2011).
[22] J. J. Peng, C. Song, B. Cui, F. Li, H. J. Mao, G. Y. Wang, and F. Pan, Appl. Phys. Lett. **107**, 182904 (2015).
[23] L. L. Tao and J. Wang, Appl. Phys. Lett. **108**, 062903 (2016).
[24] L. Bjaalie, B. Himmetoglu, L. Weston, A. Janotti, and C. G. Van de Walle, New J. Phys. **16**, 025005 (2014).
[25] P. Hansmann, X. Yang, A. Toschi, G. Khaliullin, O. K. Andersen, and K. Held, Phys. Rev. Lett. **103**, 016401 (2009).
[26] M. J. Han, C. A. Marianetti, and A. J. Millis, Phys. Rev. B **82**, 134408 (2010).
[27] E. Benckiser, M. W. Haverkort, S. Brück, E. Goering, S. Macke, A. Frañó, X. Yang, O. K. Andersen, G. Cristiani, H. U. Habermeier, A. V. Boris, I. Zegkinoglou, P. Wochner, H. J. Kim, V. Hinkov, and B. Keimer, Nat. Mater. **10**, 189 (2011).
[28] A. S. Disa, D. P. Kumah, A. Malashevich, H. Chen, D. A. Arena, E. D. Specht, S. Ismail-Beigi, F. J. Walker, and C. H. Ahn, Phys. Rev. Lett. **114**, 026801 (2015).
[29] D. Vanderbilt, Phys. Rev. B **41**, 7892(R) (1990).
[30] P. Giannozzi, S. Baroni, N. Bonini, M. Calandra, R. Car, C. Cavazzoni, D. Ceresoli, G. L. Chiarotti, M. Cococcioni, I. Dabo *et al.*, J. Phys.: Condens. Matter **21**, 395502 (2009).
[31] J. P. Perdew and A. Zunger, Phys. Rev. B **23**, 5048 (1981).
[32] S. L. Dudarev, G. A. Botton, S. Y. Savrasov, C. J. Humphreys, and A. P. Sutton, Phys. Rev. B **57**, 1505 (1998).
[33] A. Rüegg, C. Mitra, A. A. Demkov, and G. A. Fiete, Phys. Rev. B **85**, 245131 (2012).
[34] See Supplemental Material at http://link.aps.org/supplemental/10.1103/PhysRevB.98.121102 for the computational details, the TB model, the $\mathbf{k}\cdot\mathbf{p}$ Hamiltonian model, and the effects of SOC, electron-electron correlations, epitaxial strain, and quantum-well width, which includes Refs. [19,21,31–33,36–38,47].
[35] R. Pentcheva, R. Arras, K. Otte, V. G. Ruiz, and W. E. Pickett, Philos. Trans. R. Soc., A **370**, 4904 (2012).
[36] R. Winkler, *Spin-Orbit Coupling Effects in Two-Dimensional Electron and Hole Systems*, Springer Tracts in Modern Physics (Springer, Berlin, 2003).
[37] L. L. Tao, T. R. Paudel, A. A. Kovalev, and E. Y. Tsymbal, Phys. Rev. B **95**, 245141 (2017).
[38] L. L. Tao and E. Y. Tsymbal, Nat. Commun. **9**, 2763 (2018).
[39] C. Herring, Phys. Rev. **52**, 365 (1937).
[40] Y. Quan, Z. P. Yin, and W. E. Pickett, Phys. Rev. Lett. **118**, 176402 (2017).
[41] H. Weng, Y. Liang, Q. Xu, R. Yu, Z. Fang, X. Dai, and Y. Kawazoe, Phys. Rev. B **92**, 045108 (2015).
[42] C. J. Bradley and A. P. Cracknell, *The Mathematical Theory of Symmetry in Solids: Representation Theory for Point Groups and Space Groups* (Clarendon, Oxford, U.K., 1972).
[43] The basis functions for the A' and A'' representations are as follows: $|A'\rangle = c_1(|d_{x^2-y^2}\rangle_A + |d_{x^2-y^2}\rangle_B) + c_2(|d_{z^2}\rangle_A + |d_{z^2}\rangle_B)$ and $|A''\rangle = c_3(|d_{x^2-y^2}\rangle_A - |d_{x^2-y^2}\rangle_B) + c_4(|d_{z^2}\rangle_A - |d_{z^2}\rangle_B)$, where the subscripts A and B represent the two Ni sites and

$c_i (i = 1–4)$ are coefficients. Since M_z exchanges A and B sites while leaving $|d_{x^2-y^2}\rangle$ and $|d_{z^2}\rangle$ invariant, it is easy to see that $M_z|A'\rangle = +|A'\rangle$ and $M_z|A''\rangle = -|A''\rangle$. These results are confirmed by our DFT calculations.

[44] A. V. Boris, Y. Matiks, E. Benckiser, A. Frano, P. Popovich, V. Hinkov, P. Wochner, M. Castro-Colin, E. Detemple, V. K. Malik, C. Bernhard, T. Prokscha, A. Suter, Z. Salman, E. Morenzoni, G. Cristiani, H.-U. Habermeier, and B. Keimer, Science **332**, 937 (2011).

[45] R. Scherwitzl, S. Gariglio, M. Gabay, P. Zubko, M. Gibert, and J.-M. Triscone, Phys. Rev. Lett. **106**, 246403 (2011).

[46] M. Golalikhani, Q. Lei, R. U. Chandrasena, L. Kasaei, H. Park, J. Bai, P. Orgiani, J. Ciston, G. E. Sterbinsky, D. A. Arena, P. Shafer, E. Arenholz, B. A. Davidson, A. J. Millis, A. X. Gray, and X. X. Xi, Nat. Commun. **9**, 2206 (2018).

[47] C. L. Jia, X. H. Zeng, X. X. Xi, and K. Urban, Phys. Rev. B **64**, 075416 (2001).

[48] K. Momma and F. Izumi, J. Appl. Crystallogr. **44**, 1272 (2011).